Quadrupolar D–A–D diketopyrrolopyrrole-based small molecule for ternary blend polymer solar cells

Yanbin Wang, Teng Wang, Jinxing Chen, Hyung Do Kim, Penghan Gao, Biaobing Wang,* Ryo Iriguchi, Hideo Ohkita**

Dr. Y. Wang, T. Wang, J. Chen, P. Gao, Prof. B. Wang.
Jiangsu Key Laboratory of Environmentally Friendly Polymeric Materials, School of Materials Science and Engineering, Jiangsu Collaborative Innovation Center of Photovoltaic Science and Engineering, Changzhou University, Changzhou, Jiangsu, 213164, People's Republic of China.
E-mail: wangyanbin@cczu.edu.cn; biaobing@cczu.edu.cn.
Dr. H. D. Kim, R. Iriguchi, Prof. H. Ohkita
Department of Polymer Chemistry, Graduate School of Engineering, Kyoto University, Katsura, Nishikyo, Kyoto 615-8510, Japan.
E-mail: ohkita@photo.polym.kyoto-u.ac.jp.

Keywords: exciton harvesting, exciton separation, dye location, energy transfer, ternary solar cells

Abstract: A quadrupole diketopyrrolopyrrole (DPP)-based small molecule (DPP4T-Cz) was designed and synthesized to enhance absorption coefficient, and then employed as the third component to improve the light harvesting of polymer solar cells based on a blend of poly(3-hexylthiophene) (P3HT) and [6,6]-phenyl-C_{61}-butyric acid methyl ester (PCBM). Because of an enhanced absorption coefficient of more than 10^5 cm^{-1}, the photon harvesting efficiency was improved effectively in the near infrared (near-IR) range by using only a small amount of DPP4T-Cz (3.4 wt%) into the P3HT:PCBM binary blend polymer solar cells. Interestingly, the photocurrent generation was also enhanced in the visible range by the long-range energy transfer from P3HT to DPP4T-Cz molecules. As a result, the short-circuit current density (J_{SC}) and power conversion efficiency (PCE) of P3HT:PCBM:DPP4T-Cz ternary blend devices were enhanced by more than 30% compared to those of P3HT:PCBM binary control devices. These findings suggest that quadrupole DPP-based molecules are one of the effective light-harvesting materials for ternary blend polymer solar cells.

1. Introduction

Polymer solar cells have attracted more and more attention as one of the most efficient technologies for utilizing solar energy, because of their outstanding advantages such as ease of processing, potentially low cost and large scale production.[1–6] The power conversion efficiency (PCE) has been improved steadily, and increased up to more than 13% even for single-junction polymer solar cells,[7,8] but it still lags behind those of commercialized inorganic solar cells. For further improvement in the PCE, many more photons should be absorbed over a broad range from the visible to near infrared (near-IR) region. However, it is impossible to cover such a wide wavelength region of the terrestrial solar radiation by using only one or two organic materials, because the absorption bandwidth of organic materials is typically as narrow as a few hundreds of nanometers at most. As such, ternary solar cells have attracted huge attention because the third component material exhibits complementary absorption bands, which can broaden the absorption spectrum of the host binary blend.[9–15] With this strategy, the photovoltaic performances have been improved effectively, and a PCE of >14% has been reported very recently.[16]

Ternary blend polymer solar cells can be classified into sensitizer type and parallel type. In the case of the sensitization, small molecules have been employed as a third sensitizing material. For efficient ternary blend solar cells, of particular importance is a large absorption coefficient of the third small molecules. The small molecules reported so far include dye molecules and conjugated small molecules. Dye molecules typically exhibit relatively sharp and narrow absorption bands with a large absorption coefficient. For example, phthalocyanines and squaraines have an intense absorption band in a longer wavelength region compared to most of wide-bandgap conjugated polymers.[17–20] Such dye molecules are likely to form aggregates in polymer:fullerene blend films.[21–23] We therefore have employed silicon phthalocyanine derivatives with bulky

ligands for ternary blend polymer solar cells.[24–27] As a result, we found that bulky ligands can effectively suppress dye aggregation and hence improve the photocurrent generation owing to the additional absorption. Furthermore, we have shown that dye location in blends can be controlled by careful selection of ligands. More specifically, we found that hexyl ligands are compatible with poly(3-hexylthiophene) (P3HT) but benzyl ligands are compatible with a fullerene derivative (PCBM). On the basis of these findings, we demonstrated that a heterostructured dye with hexyl and benzyl ligands can most effectively improve short-circuit current density (J_{SC}) in ternary blend polymer solar cells.[28] On the other hand, conjugated small molecules exhibit relatively broad absorption bands with a modest absorption coefficient. Typically, such conjugated small molecules are compatible with conjugated donor polymers. Thus, it is required to develop conjugated small molecules with a large absorption coefficient for highly efficient ternary blend solar cells.

In this study, we have designed a conjugated small molecule with a quadrupole donor–acceptor–donor (D–A–D) structure for a sensitizer in ternary blend polymer solar cells. Such D–A–D molecular structures can enhance transition dipole moments and hence give a large absorption coefficient. Indeed, most of squaraine molecules have a large absorption coefficient because of D–A–D quadrupole structures.[17,20] Here, we selected a diketopyrrolopyrrole (DPP) moiety as an acceptor unit and a carbazole (Cz) moiety as a donor unit and synthesized a quadrupole D–A–D molecule 3,6-bis{5'-(9-(2-ethylhexyl)-9*H*-carbazol-2-yl)-[2,2'-bithiophen]-5-yl}-2,5-bis(2-ethylhexyl)-pyrrolo[3,4-*c*]pyrole-1,4-dione (DPP4T-Cz). Because of the D–A–D quadrupole structure, DPP4T-Cz exhibited a wide absorption band in the near-IR region with an absorption coefficient of more than 10^5 cm^{-1}. This DPP4T-Cz molecule was incorporated as the third sensitizer in P3HT:PCBM solar cells. Fig. 1 shows chemical structures of these three

photovoltaic materials. Consequently, the J_{SC} was increased from 10.5 to 12.9 mA cm^{-2} and hence the PCE was improved from 3 to 4% by using a small amount of DPP4T-Cz. Furthermore, the sensitization mechanism and the location of the sensitizer molecule in the active layer are also studied.

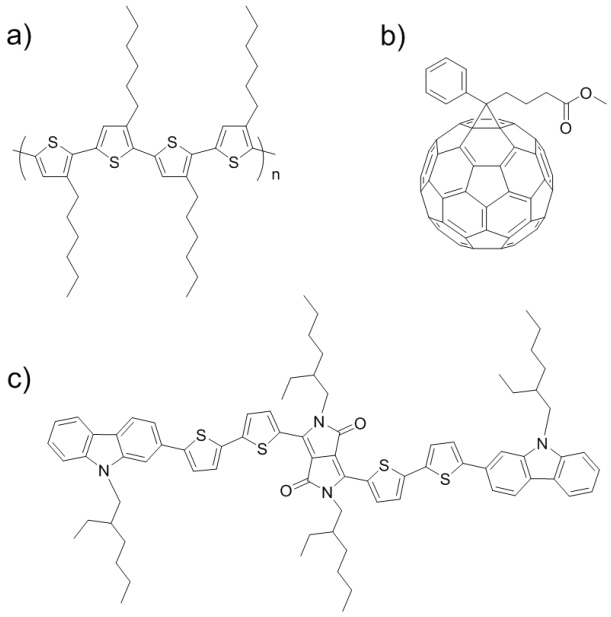

Fig. 1. Chemical structures of photovoltaic materials: a) P3HT, b) PCBM, and c) DPP4T-Cz.

2. Experimental Section

2.1. Materials

Zinc acetate dehydrate ethanolamine, 2-methoxyethanol, and P3HT were purchased from Sigma–Aldrich. A fullerene PCBM was purchased from Frontier Carbon. 3,6-Bis(5'-(trimethylstannyl)-[2,2'-bithiophen]-5-yl)-2,5-bis(2-ethylhexyl)-dihydropyrrolo[3,4-*c*]pyrrole-1, 4-dione (DPP4T) was purchased from 1-Material Inc. 2-Bromocarbazole (Cz-Br), 1-bromo-2-ethylhexane, tri(o-tolyl)phosphine ($P(o\text{-}tol)_3$), and tris(dibenzylideneacetone)dipalladium(0) ($Pd_2(dba)_3$) were purchased from Tokyo Chemical Industry. All the materials were used without further purification.

2.2. Synthesis

Scheme 1 shows a general synthetic route for the conjugated molecule DPP4T-Cz. 2-Bromo-9-(2-ethylhexyl)-9*H*-carbazole (M1) was synthesized from 2-bromocarbazole (Cz-Br) and 1-bromo-2-ethylhexane through the Hofmann alkylation reaction. 3,6-Bis{5'-(9-(2-ethylhexyl)-9*H*-carbazol-2-yl)-[2,2'-bithiophen]-5-yl}-2,5-bis(2-ethylhexyl)pyrrolo[3,4-c]pyrole-1,4-dione (DPP4T-Cz) was synthesized from M1 and DPP4T through the Stille coupling reaction. The chemical structures of intermediate M1 and the final dye molecule DPP4T-Cz have been confirmed by ^{1}H-NMR measurements.

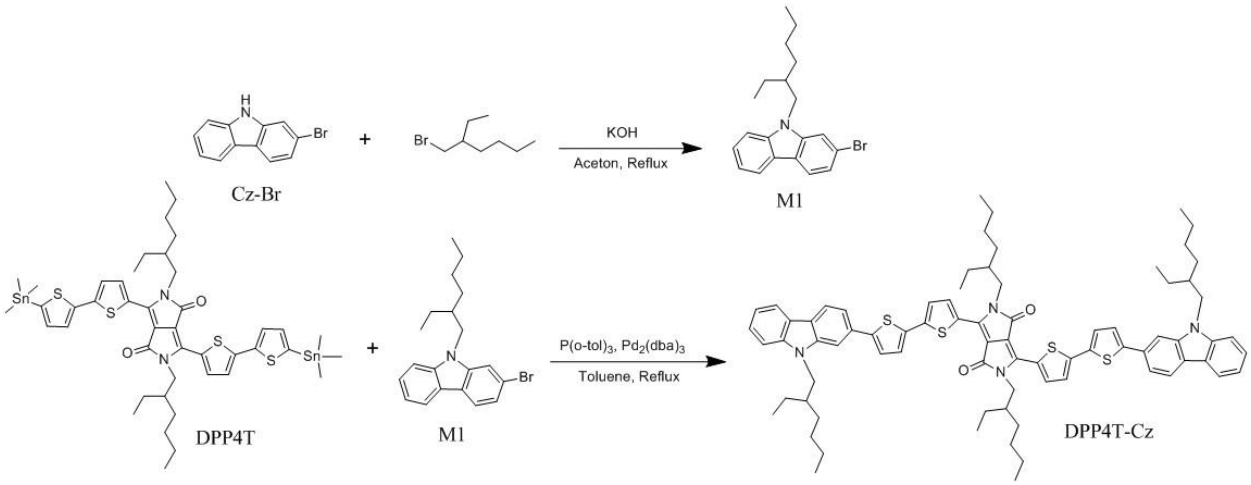

Scheme 1. Synthetic scheme of a quadrupole D−A−D molecule DPP4T-Cz.

2.2.1 Synthesis of M1

Potassium hydroxide powder (1.35 g, 24 mmol), 2-ethylhexyl bromide (4.26 mL, 24 mmol), and tetrabutylammonium hydrogen sulfate (0.2 g, 0.59 mmol) were added to Cz-Br in acetone (30 mL, 0.4 mol L^{-1}). The reaction mixture was heated slowly to reflux for overnight, and then poured into water and extracted with dichloromethane. The organic layer was washed with water and

dried over anhydrous magnesium sulfate. Further purification was performed by column chromatography on silica gel with hexane : ethyl acetate (10 : 1, v/v) as eluent, yielding 3.86 g (85%) of 2-bromo-9-(2-ethylhexyl)carbazole (M1) as colorless oil. ^{1}H-NMR (400 MHz, $CDCl_3$, δ): 8.02 (d, 1H), 7.87 (d, 1H), 7.45 (m, 2H), 7.32 (d, 1H), 7.29 (d, 1H), 7.20 (t, 1H), 4.00 (m, 2H), 2.00 (m, 1H), 1.40–1.15 (m, 8H), 0.95–0.78 (m, 6H).

2.2.2 Synthesis of DPP4T-Cz

DPP4T (200 mg, 0.197 mmol), M1 (141 mg, 0.394 mmol), $P(o\text{-}tol)_3$ (7.2 mg, 0.0236 mmol) were dissolved in 15 mL anhydrous toluene. The solution was purged with argon for 30 min, and then $Pd_2(dba)_3$ (10.8 mg, 0.0118 mmol) was added. The reaction mixture was heated slowly to reflux for 72 h, and then poured into water and extracted with dichloromethane. The organic layer was washed with water and dried over anhydrous magnesium sulfate before the solvent was evaporated. Further purification was performed by column chromatography on silica gel with hexane : dichloromethane (1 : 1, v/v) as eluent, yielding 195.5 mg (80%) of DPP4T-Cz as purple solid. ^{1}H-NMR (400 MHz, $CDCl_3$, δ): 8.92 (d, 2H), 7.77–7.72 (m, 4H), 7.57–7.54 (m, 4H), 7.40 (d, 2H), 7.32–7.28 (m, 4H), 7.20–7.14 (m, 4H), 7.03 (d, 2H), 4.32 (t, 4H), 4.23 (m, 2H), 4.08 (m, 2H), 2.05 (m, 4H), 1.80–1.55 (m, 8H), 1.50−1.18 (m, 24H), 1.06–0.82 (m, 24H).

2.3. Materials characterization

^{1}H-NMR spectra were acquired at room temperature for M1 and DPP4T-Cz on an Avance III 400M NMR (Bruker, Rheinstetten, Germany) in deuterochloroform ($CDCl_3$) containing tetramethylsilane as an internal reference. Absorption and PL spectra of blend films were investigated by spectrophotometer (Hitachi, U-3500) and spectrofluorometer (Horiba Jobin Yvon, NanoLog), respectively. Surface morphology was performed by atomic force microscopy

(Shimadzu, SPM-9600) in a tapping mode using a high resolution cantilever (MikroMasch, Hi'Res-C14/Cr-Au) with a force constant of ≈ 5 N m^{-1} and a resonance frequency of 160 kHz.

2.4. Device fabrication and characterization

Patterned indium tin oxide (ITO)-coated glass substrates with a sheet resistance of 10 ohm per square were cleaned consecutively in an ultrasonic bath containing toluene, acetone, ethanol, and deionized water for 15 min each, and then blow-dried by high purity nitrogen, finally cleaned with UV–ozone cleaner for 30 min. A precursor solution of ZnO was prepared by dissolving zinc acetate dihydrate ($Zn(CH_3COO)_2 \cdot 2H_2O$, 1 g) and ethanolamine ($NH_2CH_2CH_2OH$, 0.28 g) in 2-methoxyethanol ($CH_3OCH_2CH_2OH$, 15 mL) under vigorous stirring for one night for the hydrolysis reaction in air. The ZnO precursor solution was spin-casted on top of the ITO glass substrate at 800 rpm for 10 s and 3000 rpm for 60 s in sequence, and then were anneal at 180 °C for 1 h in air. During this process, the precursor was converted to solid-state ZnO to give transparent nanoparticle ZnO thin film, which was used as an electron-transporting layer. Subsequently, P3HT:PCBM (with and without DPP4T-Cz) solutions was spin-coated at a spin rate of 600 rpm for 60 s in the glove box, films were naturally dried under N_2 atmosphere for at least 12 h. Then, the device fabrication was completed by thermally evaporating 10-nm-thick MoO_3 and 100-nm-thick Au under vacuum at a pressure of 3×10^{-4} Pa. The effective device area was 0.07 cm^2.

The PCE was determined from *J–V* curve measurements (using a Keithley 2611B source meter) under a 1 sun, AM1.5G spectrum from a solar simulator (Oriel model 91192; 1000 W m^{-2}). The solar simulator illumination intensity was determined using a monocrystal silicon reference cell (Bunkoukeiki, BS-520). The EQE data were obtained using a solar cell spectral response measurement system (Bunkoukeiki, ECT-250D).

3. Results

3.1. Optoelectronic properties

Fig. 2 shows the absorption spectra of DPP4T-Cz in chloroform solution and in solid film on a quartz substrate. As shown in the figure, DPP4T-Cz molecules exhibit two major absorption regions at 400 nm and at 623 and 658 nm in solution. The longer absorption peaks are ascribed to the intramolecular charge transfer transition.[29,30] In the solid film state, these two peaks are observed at 660 and 725 nm, which are red-shifted by about 60 nm compared to that in solution. This red-shifted absorption suggests that the DPP4T-Cz molecules have strong intermolecular packing interaction in the solid state. More importantly, DPP4T-Cz molecules exhibit a high absorption coefficient in the near-IR region both in solution and in film state, indicating that it can be used as an effective sensitizer for improving the exciton harvesting in combination with wide-bandgap materials.

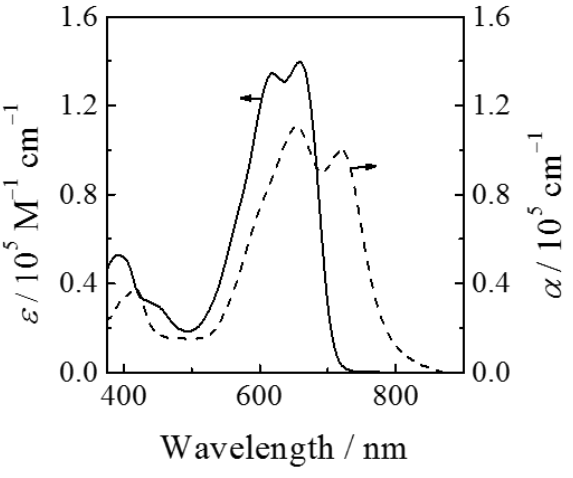

Fig. 2. Absorption spectra of DPP4T-Cz in chloroform solution (solid line) and in solid film on a quartz substrate (broken line).

As shown in Fig. 3a, P3HT exhibits a strong absorption band around 550 nm, which is complementary to the absorption spectrum of DPP4T-Cz. With the two light-harvesting materials of P3HT and DPP4T-Cz, the solar light ranging from 400 to 850 nm can be collected effectively. Furthermore, the photoluminescence (PL) spectrum of P3HT is well overlapped with the absorption spectrum of DPP4T-Cz, suggesting efficient energy transfer from P3HT to DPP4T-Cz. On the other hand, the highest occupied molecular orbital (HOMO) level of the photovoltaic materials used in this study was evaluated by photoelectron yield spectrometer (PYS) (see the Supporting Information S1), and the lowest unoccupied molecular orbital (LUMO) level was estimated from the optical bandgap and the HOMO level. As shown in Fig. 3b, the HOMO and LUMO levels of DPP4T-Cz are evaluated to be −5.2 and −3.5 eV, respectively, which are located in between those of P3HT and PCBM. It has been reported that such a cascade energy structure would be beneficial for the charge transfer at the interfaces of P3HT/DPP4T-Cz and DPP4T-Cz/PCBM.[31] In other words, there is a competition of energy transfer and charge transfer between P3HT and DPP4T-Cz at the interfaces of P3HT/DPP4T-Cz as described below.

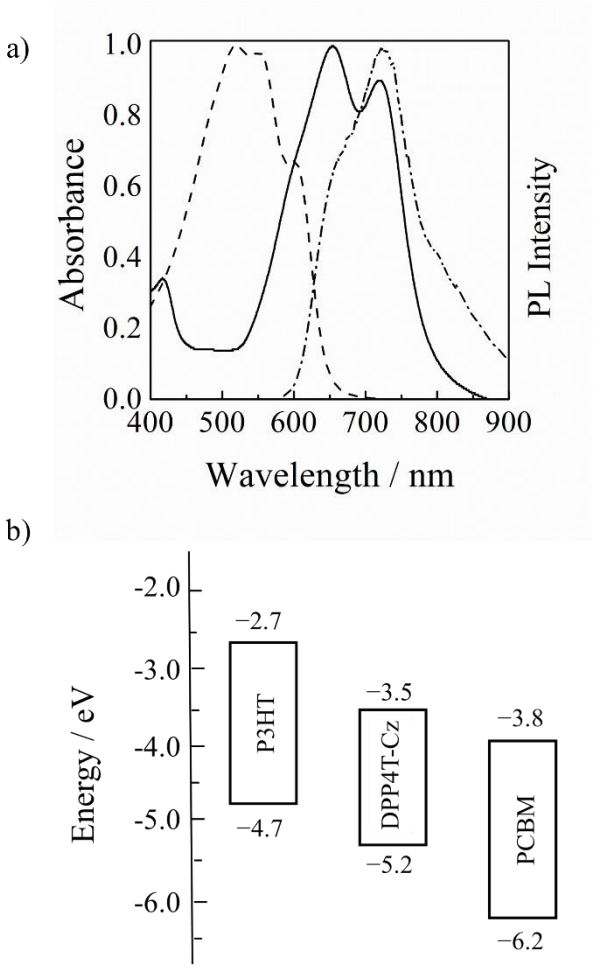

Fig. 3. a) Normalized UV–visible absorption spectra of DPP4T-Cz (solid line) and P3HT (broken line), and photoluminescence (PL) spectrum of P3HT (dashed-dotted line) in solid films. b) Energy level diagram of photovoltaic materials P3HT, DPP4T-Cz, and PCBM.

3.2. Energy transfer

To discuss the energy transfer from P3HT to DPP4T-Cz, we evaluated the Förster radius by the equation 1 assuming point-dipoles.

$$R_0^{\,6} = \frac{9000\kappa^2(\ln 10)\eta_D}{128\pi^5 n^4 N_A}\int f_D(\tilde{\nu})\varepsilon_A(\tilde{\nu})\frac{d\tilde{\nu}}{\tilde{\nu}^4} \qquad (1)$$

where κ is the orientation factor between P3HT and DPP4T-Cz ($\kappa^2 = 2/3$), η_D is the fluorescence quantum yield of P3HT in the absence of DPP4T-Cz ($\eta_D = 0.01$),[32] n is the refractive index of the medium ($n = 1.6$),[33] N_A is the Avogadro's number, f_D is the normalized donor fluorescence

spectrum, ε_A is the molar absorption coefficient of DPP4T-Cz, and $\tilde{\nu}$ is the wavenumber. On the basis of the equation 1, a Förster radius of 3.5 nm is obtained for P3HT and DPP4T-Cz. The long Förster radius indicates that there is efficient energy transfer from P3HT to DPP4T-Cz. Indeed, as shown in Fig. 4, the PL intensity of P3HT in the P3HT:DPP4T-Cz binary blend film decreased significantly while the PL intensity ascribed to DPP4T-Cz was observed clearly in the near-IR region, although the absorption of DPP4T-Cz is negligibly small at the excited wavelength. These findings suggest that P3HT excitons can be efficiently harvested through the energy transfer from P3HT to DPP4T-Cz.

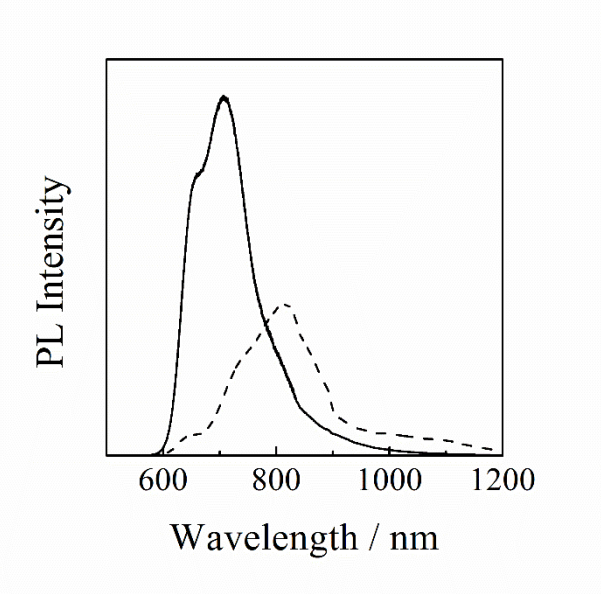

Fig. 4. Photoluminescence (PL) spectra of P3HT (solid line) and P3HT:DPP4T-Cz (broken line) with a weight ratio of 3 : 4 thin films excited at 500 nm.

3.3. *J–V* Characteristics

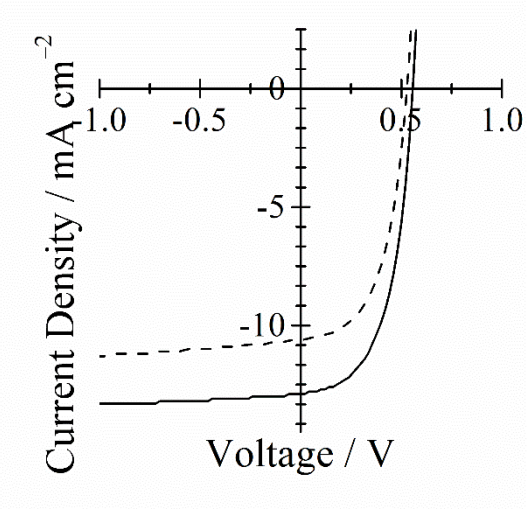

Fig. 5. The current density–voltage (*J–V*) curves of P3HT:PCBM:DPP4T-Cz ternary (solid line) and P3HT:PCBM binary (broken line) blend devices under AM1.5G simulated solar illumination.

To examine the sensitization effect of DPP4T-Cz, we fabricated binary and ternary blend polymer solar cells with an inverted layered structure of ITO/ZnO/active layers/MoO_3/Au under the same conditions. As shown in Fig. 5, the P3HT:PCBM binary control device gave a PCE of 3% with J_{SC} of 10.5 mA cm^{-2}, V_{OC} of 0.53 V, and FF of 0.54. With addition of only 3.4 wt% of DPP4T-Cz molecules into the binary blends, the photovoltaic performance of P3HT:PCBM:DPP4T-Cz ternary blend devices was improved significantly as summarized in Table 1. It is noteworthy that the J_{SC} was improved obviously up to 12.9 mA cm^{-2}. In addition, the fill factor (FF) was slightly improved from 0.54 for the binary control device to 0.56 for the P3HT:PCBM:DPP4T-Cz ternary blend device, suggesting that charge transport in ternary blends is better than in binary blends. On the other hand, the open-circuit voltage (V_{OC}) of P3HT:PCBM:DPP4T-Cz ternary blend devices remained the same as those of the binary devices. Hence the PCE was improved from 3.0% for the P3HT:PCBM binary control devices to 4.0% for the P3HT:PCBM:DPP4T-Cz ternary blend devices. Further addition of DPP4T-Cz rather decreased the photocurrent generation and hence degraded the overall photovoltaic performance.

A similar sensitization effect was found for another ternary blend solar cell based on poly[5,5'-bis(2-butyloctyl)-(2,2'-bithiophene)-4,4'-dicarboxylate-alt-5,5'-2,2'-bithiophene] (PDCBT), PCBM, and DPP4T-Cz. In this case, the J_{SC} was increased from 10.2 to 12.4 mA cm^{-2}, thus PCE was improved by 17% from 5.2% for PDCBT/PCBM binary blend solar cells to 6.1% for PDCBT/PCBM/DPP4T-Cz without further optimization (see the Supporting Information S2). This finding suggests that our DPP4T-Cz is a versatile sensitizer for improving the efficiency of polymer solar cells.

Table 1. Device parameters of ternary blend polymer solar cells.

P3HT : PCBM : DPP4T-Cz	J_{SC} / mA cm^{-2}	V_{OC} / V	FF	PCE / %
20 : 20 : 0 (0 wt%)	10.5	0.53	0.54	3.00
20 : 20 : 0.7 (1.7 wt%)	11.3	0.54	0.56	3.42
20 : 20 : 1.4 (3.4 wt%)	12.9	0.56	0.56	4.04
20 : 20 : 2.1 (5.0 wt%)	11.7	0.54	0.51	3.22

3.4. External quantum efficiency (EQE) spectra

To address the origin of the improvement in J_{SC}, we measured the external quantum efficiency (EQE) spectra of P3HT:PCBM binary control and P3HT:PCBM:DPP4T-Cz ternary blend devices (see the Supporting Information S3). With the addition of 3.4 wt% DPP4T-Cz into the binary blend, the EQE signal was observed in the near-IR region for the ternary blend polymer solar cells, which is consistent with the improved absorption as shown in Fig. 6a. Interestingly, the EQE signal ascribed to P3HT was also enhanced at around 550 nm from 61 to 72% as shown in Fig. 6b, although there is no difference in the absorption between P3HT:PCBM binary and P3HT:PCBM:DPP4T-Cz ternary blend films, as reported previously.[24,34] This is probably

because there is efficient energy transfer from P3HT to DPP4T-Cz, which can collect the P3HT exciton lost in the P3HT:PCBM binary blend. On the other hand, as shown in Fig. 6a, the vibronic band at around 600 nm was observed in the both blend films, indicating that P3HT crystalline domains are not disturbed in the P3HT:PCBM:DPP4T-Cz ternary blend films. This is consistent with almost the same hole mobility and surface morphology observed for both binary and DPP4T-Cz blended ternary films (see the Supporting Information S4 and S5).

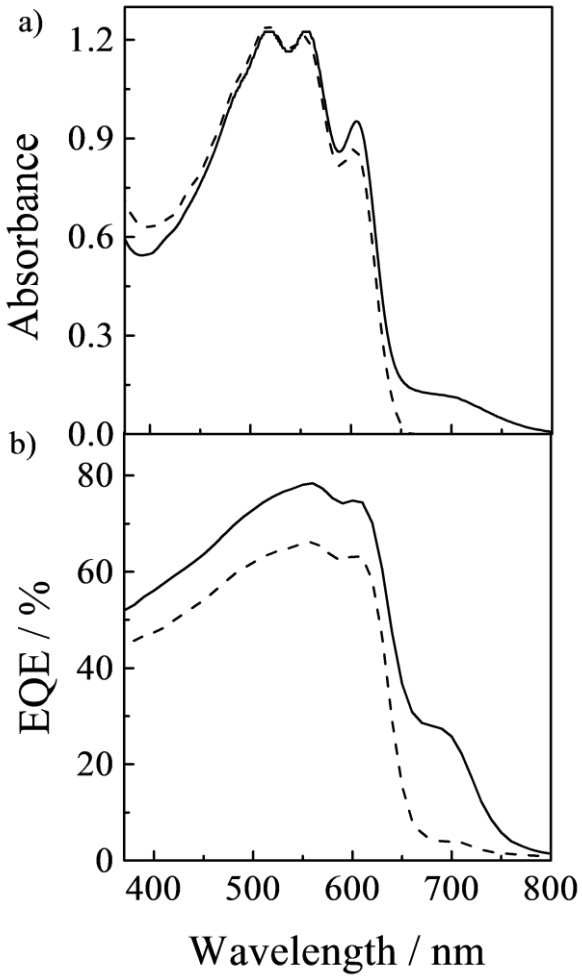

Fig. 6. a) Thin film UV–visible absorption spectra and b) external quantum efficiency (EQE) characteristics of P3HT:PCBM binary (broken line) and P3HT:PCBM:DPP4T-Cz ternary (solid line) blend devices.

4. Discussion

As mentioned above, the photovoltaic performance of P3HT:PCBM:DPP4T-Cz ternary blend devices has been improved compared with P3HT:PCBM binary control devices. There are two reasons for this: one is the direct light-harvesting ascribed to DPP4T-Cz, and the other is the improved exciton-harvesting of P3HT due to the energy transfer.

Firstly, we focus on the high absorption coefficient molecule of DPP4T-Cz. As shown in Figs. 6a and 6b, with the addition of only 3.4 wt% DPP4T-Cz into the binary blend, the photocurrent generation was improved obviously in the near-IR region. By integrating the product of the AM1.5G solar spectrum and the absorption spectrum of DPP4T-Cz, the direct photocurrent generated by DPP4T-Cz is estimated to be 0.6 mA cm^{-2}. Furthermore, the internal quantum efficiency (IQE) of the P3HT:PCBM:DPP4T-Cz ternary blend device was estimated to be 93% from the EQE and absorption spectra at 710 nm, suggesting that more than 93% of DPP4T-Cz molecules are located at the interface of P3HT/PCBM, this is because that only DPP4T-Cz molecules at the interface can contribute to the photocurrent as shown in Fig. 7. In order to figure out such spontaneous location of DPP4T-Cz molecules in ternary blend films, we measured surface energy (γ) of P3HT, PCBM, and DPP4T-Cz by the contact angle method. As a result, we found that the surface energy is estimated to be 18.9 mJ m^{-2} for P3HT, 22.0 mJ m^{-2} for DPP4T-Cz, and 30.6 mJ m^{-2} for PCBM as summarized in Table 2. Consequently, a wetting coefficient (ω) derived from the surface energy was estimated to be 0.46 for DPP4T-Cz in the P3HT:PCBM:DPP4T-Cz ternary blend film from Neumann's and Young's equations.[35] Previously, it has been reported that if $-1 < \omega < 1$, the third component material would be located at the interface of the host binary blend.[28,36] These results support that the location of DPP4T-Cz plays a key role in the sensitization of ternary blends.

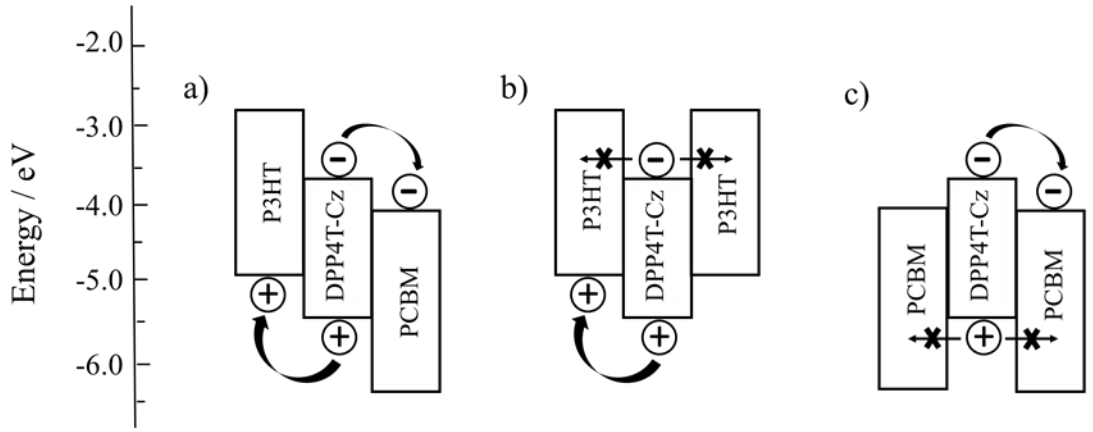

Fig. 7. Charge transfer of DPP4T-Cz molecules a) at the interfaces of P3HT and PCBM, b) in the domains of P3HT, and c) in the domains of PCBM, respectively.

Table 2. Surface energy of P3HT, DPP4T-Cz, and PCBM.

	P3HT	DPP4T-Cz	PCBM
γ / mJ m^{-2}	18.9	22.0	30.6

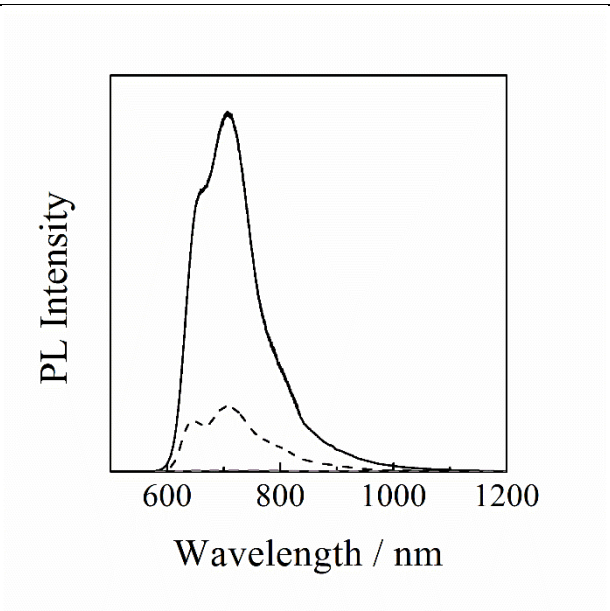

Fig. 8. Photoluminescence (PL) spectra of P3HT (black solid line), P3HT:PCBM with a weight ratio of 1 : 1 (black broken line), and P3HT:PCBM:DPP4T-Cz (grey solid line) ternary blend films excited at 500 nm.

Now, we focus on the energy transfer from P3HT to DPP4T-Cz. As shown in Fig. 8, although the PL intensity of P3HT decreased significantly for the P3HT:PCBM binary blend film with a weight ratio of 1 : 1, 20% of P3HT excitons radiatively were deactivated to the ground state before arriving at the interface because of the large P3HT domains. Typically, an exciton diffusion length of conjugated polymers has been reported to be only about 10 nm,[37,38] which limits the exciton diffusion efficiency, especially for highly crystalline polymers. On the other hand, it has been confirmed that the exciton diffusion efficiency can be improved through the long-range energy transfer.[39] Indeed, with the addition of 3.4 wt% of DPP4T-Cz molecules in the P3HT:PCBM binary blend, the P3HT excitons was quenched completely. The improved exciton diffusion efficiency is useful for achieving a higher photocurrent in the visible region. By integrating the product of the AM1.5G solar spectrum and the absorption spectrum of P3HT, the photocurrent ascribed to the energy transfer is estimated to be 1.8 mA cm^{-2}. In other words, the photocurrent ascribed to the energy transfer is three times as high as that ascribed to the direct light harvesting from DPP4T-Cz.

Finally, we note that DPP4T-Cz can be easily employed as a monomer building unit in DPP-based conjugated polymers. This is one of the advantages over dye molecules such as phthalocyanines and squaraines. In this study, the optimized loading concentration is as small as 3.4 wt%, which is similar to that reported for dye molecules in ternary blend polymer solar cells. This is partly because DPP4T-Cz is compatible with P3HT rather than PCBM and hence would be located in P3HT domains under high loading conditions as reported previously.[34,36] This limitation would be overcome by using a conjugated polymer based on DPP4T-Cz unit, which can be served as the third component in parallel-type ternary blend polymer solar cells.

5. Conclusion

In summary, a quadrupole molecule DPP4T-Cz with a high absorption coefficient was designed and incorporated into the host binary blend of P3HT and PCBM. The light harvesting was improved in the near-IR range by the additional absorption and the exciton harvesting was improved in the visible region by the long-range energy transfer even though the concentration of the third component was as low as 3.4 wt%. This is because the conjugated small molecule exhibits a high absorption coefficient due to transition dipole moments enhanced by such D–A–D molecular structures. We believe that this building block is generally applicable to design conjugated polymers with a high absorption coefficient for organic optoelectronic devices.

Acknowledgments

This work was partly supported by the Natural Science Foundation of Jiangsu Province (BK20160280), Double Plan of Jiangsu Province, and the Japan Science and Technology Agency (JST) ALCA program (Solar Cell and Solar Energy Systems).

Appendix A. Supplementary data

Supplementary data related to this article can be found at the web of the ScienceDirect Online Library.

References

1. Hedley GJ, Ruseckas A, Samuel ID. Light harvesting for organic photovoltaics. Chem Rev 2017;117:796-837.

2. Mateker WR, McGehee MD. Ternary polymer solar cells based on two acceptors and one donor for achieving 12.2% efficiency. Adv Mater 2017;29:1604059.

3. Zhang K, Hu Z, Sun C, Wu Z, Huang F, Cao Y. Toward solution-processed high-performance polymer solar cells: from material design to device engineering. Chem Mater 2017; 29:141-8.

4. Holliday S, Li Y, Luscombe CK. Recent advances in high performance donor-acceptor polymers for organic photovoltaics. Prog Polym Sci 2017;70:34-51.

5. Luo G, Ren X, Zhang S, Wu H, Choy WC, He Z, Cao Y. Recent advances in organic photovoltaics: device structure and optical engineering optimization on the nanoscale. Small 2016;12:1547-71.

6. Mazzio KA, Luscombe CK. The future of organic photovoltaics. Chem Soc Rev 2015;44: 78-90.

7. Xu X, Yu T, Bi Z, Ma W, Li Y, Peng Q. Realizing over 13% efficiency in green-solvent-processed nonfullerene organic solar cells enabled by 1,3,4-thiadiazole-based wide-bandgap copolymers. Adv Mater 2018;30:1703973.

8. Zhao W, Li S, Yao H, Zhang S, Zhang Y, Yang B, Hou J. Molecular optimization enables over 13% efficiency in organic solar cells. J Am Chem Soc 2017;139:7148-51.

9. Lu H, Xu X, Bo Z. Perspective of a new trend in organic photovoltaic: ternary blend polymer solar cells. Sci China Mater 2016;59:444-58.

10. An Q, Zhang F, Zhang J, Tang W, Deng Z, Hu B. Versatile ternary organic solar cells: a critical review. Energy Environ Sci 2016;9:281-322.

11. Lu L, Kelly MA, You W, Yu L. Status and prospects for ternary organic photovoltaics. Nat Photon 2015;9:491-500.

12. Huang H, Yang L, Sharma B. Recent advances in organic ternary solar cells. J Mater Chem A 2017:5:9418-20.

13. Li H, Lu K, Wei Z. Polymer/small molecule/fullerene based ternary solar cells. Adv Energy Mater 2017;7:1602540.

14. Ameri T, Khoram P, Min J, Brabec CJ. Organic ternary solar cells: a review. Adv Mater 2013;25:4245-66.

15. Savoie BM, Dunaisky S, Marks TJ, Ratner MA. The scope and limitations of ternary blend organic photovoltaics. Adv Energy Mater 2014:5:1400891.

16. Xiao Z, Jia X, Ding L. Ternary organic solar cells offer 14% power conversion efficiency. Sci Bull 2017;62:1562-64.

17. Xiao L, Gao K, Zhang Y, Chen X, Hou L, Cao Y, Peng X. A complementary absorption small molecule for efficient ternary organic solar cells. J Mater Chem A 2016;4:5288-93.

18. Mohsin HAA, Mineart KP, Armstrong DP, Shafei AE, Spontak RJ. Quasi-solid-state dye-sensitized solar cells containing a charged thermoplastic elastomeric gel electrolyte and hydrophilic/phobic photosensitizers. Sol RRL 2018:2:1700145.

19. Bucher L, Desbois N, Harvey PD, Sharma GD, Gros CP. Porphyrins and BODIPY as building blocks for efficient donor materials in bulk heterojunction solar cells. Sol RRL 2017;1:1700127.

20. Park J, Barolo C, Sauvage F, Barbero N, Benzi C, Quagliotto P, Coluccia S, Censo DD, Gratzel M, Nazeeruddin MK, Viscardi G. Symmetric vs. asymmetric squaraines as photosensitisers in mesoscopic injection solar cells: a structure-property relationship study. Chem Commun 2012;48:2782-84.

21. Zhu L, Wang R, Qiao J, Wu F. Enhanced photovoltaic performance of ternary solar cells by doping a new squaraine derivative. Dyes Pigments 2016:132;20-6.

22. Peukert A, Roca LV, Scherer M, Lovrincic R, Ramanan C, Chanaewa A, Hauff EV. Controlled morphology of ZnO nanorods for electron transport in squaraine bulk-hetero junction solar cells with thick active layers. Sol RRL 2017;1:1700132.

23. Stylianakis MM, Konios D, Viskadouros G, Vernardou D, Katsarakis N, Koudoumas E, Anastasiadis SH, Stratakis E, Kymakis E. Ternary organic solar cells incorporating zinc phthalocyanine with improved performance exceeding 8.5%. Dyes Pigments 2017;146:408-13.

24. Honda S, Nogami T, Ohkita H, Benten H, Ito S. Improvement of the light-harvesting efficiency in polymer/fullerene bulk heterojunction solar cells by interfacial dye modification. ACS Appl Mater Interfaces 2009;1:804-10.

25. Honda S, Ohkita H, Benten H, Ito S. Multi-colored dye sensitization of polymer/fullerene bulk heterojunction solar cells. Chem Commun 2010;46:6596-8.

26. Xu H, Wada T, Ohkita H, Benten H, Ito S. Dye sensitization of polymer/fullerene solar cells incorporating bulky phthalocyanines. Electrochim Acta 2013;100:214-9.

27. Honda S, Ohkita H, Benten H, Ito S. Selective dye loading at the heterojunction in polymer/ fullerene solar cells. Adv Energy Mater 2011;1:588-98.

28. Xu H, Ohkita H, Tamai Y, Benten H, Ito S. Interface engineering for ternary blend polymer solar cells with a heterostructured near-IR dye. Adv Mater 2015;27:5868-74.

29. Yu D, Liu Y, Xiao M, Fan Q, Su W, Li X, Tan H, Wang Y, Yang R, Zhu W. Synthesis and photovoltaic performance of DPP-based small molecules with tunable energy levels by altering the molecular terminals. Dyes Pigments 2016;125:151-8.

30. Tamayo AB, Walker B, Nguyen TQ. A low band gap, solution processable oligothiophene with a diketopyrrolopyrrole core for use in organic solar cells. J Phys Chem C 2008;112:11545-

31. Groves C. Suppression of geminate charge recombination in organic photovoltaic devices with a cascaded energy heterojunction. Energy Environ Sci 2013;6:1546-51.

32. Kim Y, Bradley DDC. Bright red emission from single layer polymer light-emitting devices based on blends of regioregular P3HT and F8BT. Curr Appl Phy 2005;5:222-6.

33. Mor GK, Kim S, Paulose M, Varghese OK, Shankar K, Basham J, Grimes CA. Visible to near-infrared light harvesting in TiO_2 nanotube array-P3HT based heterojunction solar cells. Nano Lett 2009;9:4250-7.

34. Wang Y, Ohkita H, Benten H, Ito S. Highly efficient exciton harvesting and charge transport in ternary blend solar cells based on wide- and low-bandgap polymers. Phys Chem Chem Phys 2015;17:27217-24.

35. Sumita M, Sakata K, Asai S, Miyasaka K, Nakagawa H. Dispersion of fillers and the electrical conductivity of polymer blends filled with carbon black. Polym Bull 1991;25:265-71.

36. Wang Y, Zheng B, Tamai Y, Ohkita H, Benten H, Ito S. Dye sensitization in the visible region for low-bandgap polymer solar cells. J Electrochem Soc 2014;161:D3093-6.

37. Wang Y, Benten H, Ohara S, Kawamura D, Ohkita H, Ito S. Measurement of exciton diffusion in a well-defined donor/acceptor heterojunction based on a conjugated polymer and cross-linked fullerene derivative. ACS Appl Mater Interfaces 2014;6:14108-15.

38. Menke SM, Holmes RJ. Exciton diffusion in organic photovoltaic cells. Energy Environ Sci 2014;7:499-512.

39. Wang Y, Ohkita H, Benten H, Ito S. Efficient exciton harvesting through long-range energy transfer. ChemPhysChem 2015;16:1263-7.

Supporting Information

Quadrupolar D–A–D diketopyrrolopyrrole-based small molecule for ternary blend polymer solar cells

Yanbin Wang,[a,] Teng Wang,[a] Jinxing Chen,[a] Hyung Do Kim,[b] Penghan Gao,[a] Biaobing Wang,[a,]* Ryo Iriguchi,[b] Hideo Ohkita,[b,]**

[a)] Jiangsu Key Laboratory of Environmentally Friendly Polymeric Materials, School of Materials Science and Engineering, Jiangsu Collaborative Innovation Center of Photovolatic Science and Engineering, Changzhou University, Changzhou, Jiangsu, 213164, People's Republic of China.

[*]*E-mail: wangyanbin@cczu.edu.cn*

[b)] Department of Polymer Chemistry, Graduate School of Engineering, Kyoto University, Katsura, Nishikyo, Kyoto 615-8510, Japan.

[*]*E-mail: ohkita@photo.polym.kyoto-u.ac.jp*

1. Photoelectron yield spectroscopy (PYS)

The ionization potential of the sample films was measured with a photoelectron yield spectrometer (PYS) (Riken Keiki, AC-3). The sample films were fabricated by spin-coating from a chlorobenzene solution onto a cleaned ITO substrate. The ionization potential energy was estimated from a threshold energy of the cubic root of the photoelectron yield plotted against the incident photon energy.

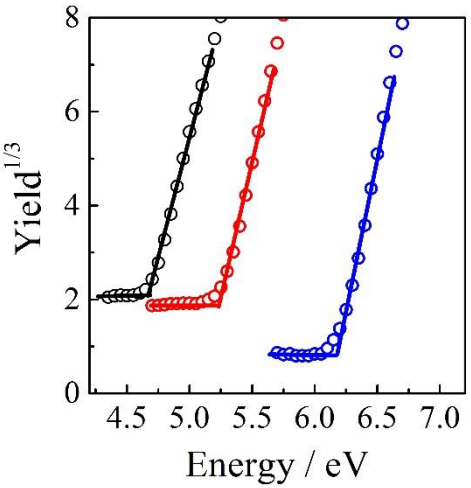

Fig. S1. The photoemission yield spectra of P3HT (black circles), DPP4T-Cz (red circles), and PCBM (blue circles) neat films.

2. ***J–V* Characteristics**

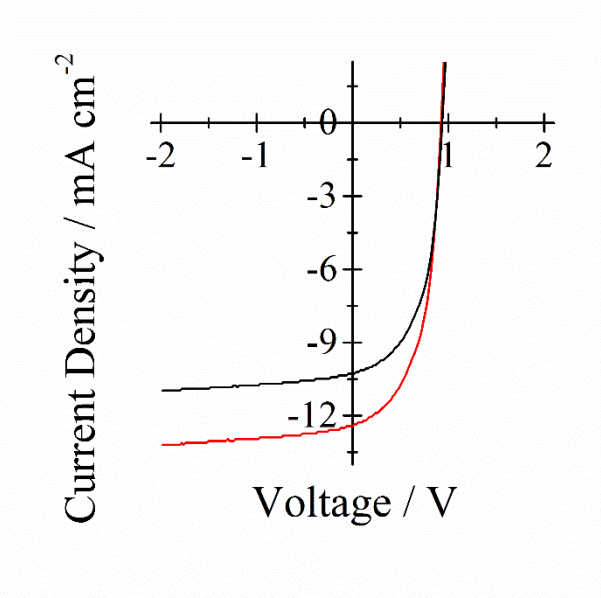

Fig. S2. The current density–voltage (*J–V*) curves of PDCBT:PCBM binary blend with a weight ratio of 10:10 (black line) and PDCBT:PCBM:DPP4T-Cz ternary blend with a weight ratio of 10:10:1.5 devices under AM1.5G simulated solar illumination.

3. EQE spectra

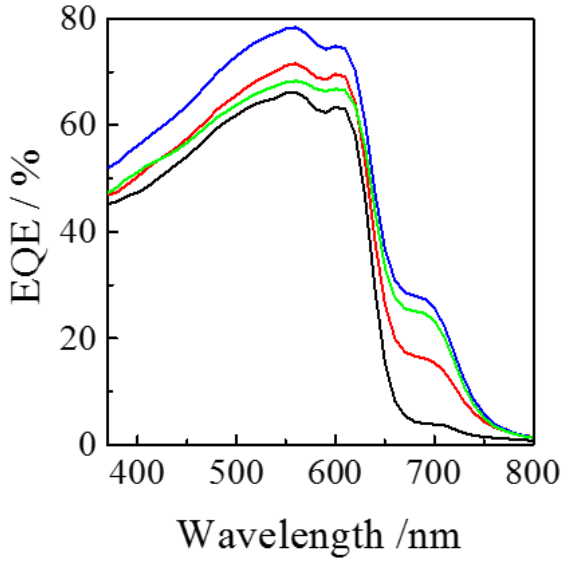

Fig. S3. EQE spectra of P3HT:PCBM binary blend (black line), P3HT:PCBM:DPP4T-Cz ternary blend with different compositions: P3HT : PCBM : DPP4T-Cz = 20 : 20 : 0.7 (green line), 20 : 20 : 1.4 (blue line), and 20 : 20 : 2.1 (red line).

4. Charge mobility

Charge carrier mobilities were evaluated from *J*–*V* characteristics using the space-charge-limited current (SCLC) method with the Mott-Gurney equation for the current density J_{SCLC} expressed as $J_{SCLC} = \frac{9}{8}\varepsilon_0\varepsilon_r\mu\frac{V^2}{L^3}$, where ε_r is the dielectric constant of the film ($\varepsilon_r = 3$ was assumed), and *L* is the thickness of the active layer. The mobilities were evaluated from SCLC currents measured for the hole-only devices with a structure of ITO/PEDOT:PSS/active layer/Au.

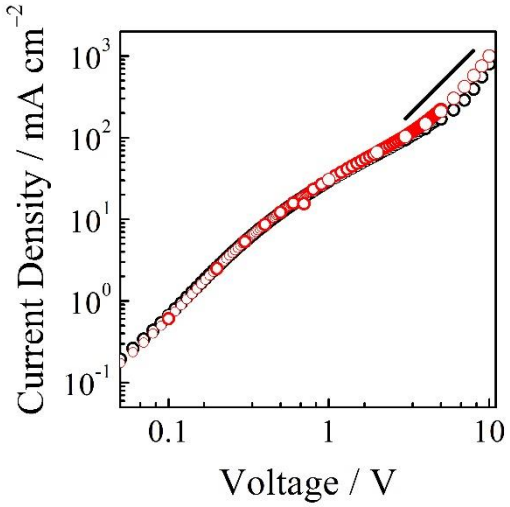

Fig. S4. *J*–*V* characteristics of hole-only devices with a P3HT:PCBM binary blend (black circles) and P3HT:PCBM:DPP4T-Cz ternary blend (red circles) as an active layer. The solid line represents a line with a slope of two.

Table S1. Hole mobilities of binary and ternary blend films.

	P3HT:PCBM	P3HT:PCBM:DPP4T-Cz
μ_h / 10^{-4} cm^2 V^{-1} s^{-1}	7.9	9.2

5. Morphology

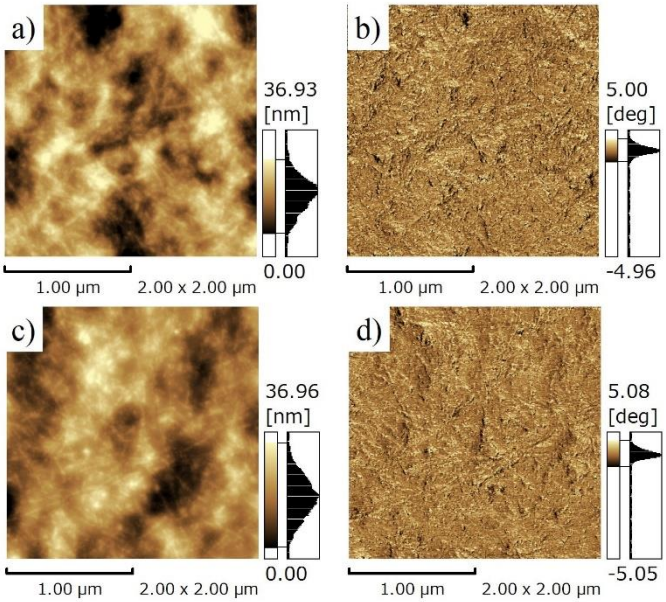

Fig. S5. AFM height (a, c) and (b, d) phase images for P3HT:PCBM binary blend (a, b) and P3HT:PCBM:DPP4T-Cz ternary blend (c, d) films.